An Inversion-Charge Analytical Model for Square Gate-All-Around MOSFETs

Enrique Moreno Pérez, Juan Bautista Roldán Aranda, Francisco J. García Ruiz, Domingo Barrera Rosillo, María José Ibáñez Pérez, Andrés Godoy, *Member, IEEE*, and Francisco Gámiz

***Abstract*—A new approach to the analytical solution of the 2-D Poisson equation including the inversion-charge density in undoped square gate-all-around metal–oxide–semiconductor field-effect transistors has been developed. We have obtained functions with different degrees of complexity to calculate the electric potential in the devices under study. The results obtained are compared with the data simulated by solving the Poisson equation numerically. A good fit is achieved both for the electric potential and the inversion charge, which are calculated by means of Gauss's law.**

***Index Terms*—MOSFETs, semiconductor device modeling, silicon devices, thin film devices.**

I. Introduction

MULTIPLE-GATE MOSFETs are considered key devices in the current scaling landscape imposed by Moore's law (which, for the near future, considers channel lengths of 22 nm and below). These structures show promising possibilities related to the control of short-channel effects (SCEs), the achievement of ideal subthreshold swing values, and the maximization of the $I_{\rm on}/I_{\rm off}$ ratio, as well as lower parasitic capacitances compared with their conventional counterparts [1]–[3]. The use of undoped substrates (due to their intrinsic low SCEs) facilitates the efforts of process engineers to deal with variability issues (i.e., random impurity effects in the active region of the transistor are known to be one of the most important sources of statistical variability), which present significant difficulties in the scaling process due to the dispersion of fundamental parameters such as the threshold voltage and the subthreshold slope [4]–[6]. In particular, gate-all-around (GAA) MOSFETs present some promising and unique features to be considered for future low-power and radio-frequency analog technologies [5], [7].

Both square and cylindrical GAA MOSFETs are currently under intense study from the simulation and modeling viewpoints [8]–[13]. The analytical description of cylindrical GAA MOSFETs is simpler, i.e., due to the symmetry of the structure around the rotation angle, which allows a 1-D description accounting for just the radial component [8]–[10], [13]. However, unlike their cylindrical counterparts, square GAA MOSFETs have not been described yet analytically in depth due to their complex geometry, making new modeling strategies necessary.

Some authors have proposed recently an approach based on Fourier series expansions of the electric potential in the device [14]. However, in this paper, we have developed a different technique, which provides a more compact approach, for building analytical functions to model the electric potential in square GAA MOSFETs. These functions are solutions of the 2-D Poisson equation, where the charge density in the silicon channel includes the inversion charge. In this respect, the approach that we are following is much more accurate than others presented previously [11], which do not include the inversion charge for the calculation of the electric potential (these calculations were thought to analyze the potential distribution for threshold-voltage modeling purposes, i.e., at the onset of the inversion operation region, where the inversion charge can be neglected reasonably). The inclusion of the inversion charge in our calculations makes feasible the modeling of the most important operation regions (from the subthreshold regime to the strong-inversion regime). We also propose a couple of functions to model the electric potential of square GAA MOSFETs. The use of these functions faces us with the usual compact-modeling tradeoff: complexity versus accuracy. In this regard, we will discuss the pros and cons of the functions we make use of. We will also calculate the inversion charge (by means of Gauss's law) and compare the results with simulation data obtained with a 2-D simulator developed for this purpose [15], [16].

Inversion-charge modeling is the starting point for drain current and capacitance models necessary for the development of compact models with emphasis on circuit simulation. The mobility models that are included usually in these compact models also depend on the inversion charge; therefore, obvious interest exists in developing accurate models of this magnitude.

This paper is organized as follows. in Section II, we describe briefly the main features of the numerical simulator used. We deal with the electric potential modeling in Section III, and the calculation and the modeling of the inversion charge, as well as

Manuscript received January 10, 2011; revised May 20, 2011; accepted May 25, 2011. Date of publication July 25, 2011; date of current version August 24, 2011. This work was supported in part by the Junta de Andalucía under Research Project P08-TIC-3580 and Research Project P09-TIC1899, by the Government of Spain under Research Project TEC2008-06758-C02-01 and Research Project FIS2008-05805, by the European platform for low-power applications on Silicon-on-Insulator Technology (EUROSOI+) Thematic Network under Grant FP7-ICT-216373, and by the Silicon-Based Nanostructures and Nanodevices for Long Term Nanoelectronics Applications Network of Excellence under Grant FP7-NOE-216171. The review of this paper was arranged by Editor V. R. Rao.

E. Moreno Pérez, J. B. Roldán Aranda, F. J. García Ruiz, A. Godoy, and F. Gámiz are with the Department of Electronics and Computer Technology, Faculty of Science, University of Granada, 18071 Granada, Spain (e-mail: jroldan@ugr.es).

D. Barrera Rosillo and M. J. Ibáñez Pérez are with the Department of Applied Mathematics, Faculty of Science, University of Granada, 18071 Granada, Spain.

Color versions of one or more of the figures in this paper are available online at http://ieeexplore.ieee.org.

Digital Object Identifier 10.1109/TED.2011.2159222

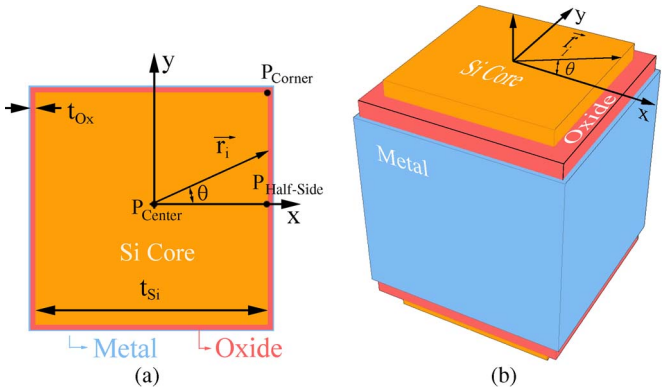

Fig. 1. Cross section and 3-D geometry of the square GAA MOSFET under study.

some discussion, are presented in Section IV. Finally, the main conclusions are given in Section V.

II. Simulator Description

The simulation data presented in this paper have been obtained with a simulator developed within our research group [15], [16]. The geometry and the cross section of the GAA MOSFET studied is shown in Fig. 1. It can be seen that the gate surrounds completely the square silicon channel where conduction takes place. In this paper, long-channel devices are considered; in this respect, only the 2-D cross section of the device is simulated. Further effects such as SCEs will be included in future versions of the model.

The simulator solves the 2-D Poisson equation in the cross section of the device, making use of finite elements for the discretization. More details of the code can be found in [15] and [16]. In all the simulated devices, we considered an undoped substrate and a metal gate with a work function of 4.63 eV. The t_{Si} (i.e., the silicon bulk width) values considered in this paper were 10 and 20 nm, and parameter t_{Ox} (i.e., the thickness of the insulator layer SiO_2) was 1.5 nm.

A quantum description would be needed to model accurately the behavior of the devices considered in this paper, although their size makes structural confinement less relevant than in thinner devices [17], [18]. However, the degree of complexity required for a compact-modeling approach of the self-consistent analytical solution of the 2-D Poisson and Schrödinger equations would make the problem inaccessible. For this reason, we considered that a description based on a classical electrical potential function could be a reasonable first step in modeling the behavior of GAA MOSFETs, i.e., in line with the reasoning in [17] and [18]. Therefore, although the simulator accounts for quantization, a classical approach has been used here for comparison with the models presented below. Quantum effects can be added as correction terms in future studies to maintain the coherence of the approach we are following.

III. Electric Potential Modeling

The electric potential in the silicon channel of the device shown in Fig. 1 has been obtained by solving the 2-D Poisson equation, making use of the coordinate system sketched in the same figure. In our calculations, we have accounted only for electron charge: Holes are neglected, considering that $q\psi/kT > 1$, and the depletion charge is also neglected due to the use of an undoped or lightly doped silicon core, i.e., N_A or $N_D \ll n$. For the calculation of electric potential, the Poisson equation holds

$$\frac{\partial^2\psi(x,y)}{\partial x^2}+\frac{\partial^2\psi(x,y)}{\partial y^2}=\frac{-\rho(x,y)}{\epsilon_{\mathrm{Si}}} =\frac{qn(x,y)}{\epsilon_{\mathrm{Si}}}=\frac{q}{\epsilon_{\mathrm{Si}}}n_i e^{\frac{q\psi(x,y)}{KT}} \quad (1)$$

where q is the electronic charge, ϵ_{Si} is the silicon permittivity, K is the Boltzmann's constant, T stands for the temperature, and n_i stands for the intrinsic electron density. The Poisson equation solutions can be built by using (see Appendix A)

$$\psi(x,y)=\frac{1}{\beta}\ln\left(\frac{8\phi'(z)\phi'^{*}(z)}{\alpha\beta\left(1-\phi(z)\phi^{*}(z)\right)^2}\right). \quad (2)$$

In the previous equation, $\psi(x,y)$ is the electric potential, and the complex function $\phi(z)$ can be described as $\phi(z)=u(x,y)+\imath v(x,y)$. In order to determine completely the expression of the electric potential, we considered the boundary conditions along the perimeter of the silicon channel, which was at the silicon–insulator interface. These boundary conditions can be expressed as follows:

$$\overrightarrow{\nabla}\psi(P_{i,\,\mathrm{Boundary}})\cdot\hat{r_i}=\Omega\frac{V_G-\Delta\phi_{\mathrm{MS}}-\psi(P_{i,\,\mathrm{Boundary}})}{\frac{t_{\mathrm{Ox}}}{\cos\theta}} \quad (3)$$

where $\hat{r_i}$ are unitary vectors with their initial point at the center of the silicon channel and their direction sweeping different points at the insulator–semiconductor interface $P_{i,\,\mathrm{Boundary}}$ (see Fig. 1) with $\theta=\arctan(|r_{\mathrm{iy}}|/|r_{\mathrm{ix}}|)$, $\Omega=\epsilon_{\mathrm{Ox}}/\epsilon_{\mathrm{Si}}$ is the ratio between the oxide and silicon permittivities, $\Delta\phi_{\mathrm{MS}}$ is the difference between the metal and semiconductor work functions, V_G is the gate voltage, and $\psi(P_{i,\,\mathrm{Boundary}})$ is the value of electric potential at $P_{i,\,\mathrm{Boundary}}$. The evaluation of (3) at the two representative points of the silicon–insulator interface (i.e., placed in the middle of the silicon channel side $P_{\mathrm{Half-side}}=(t_{\mathrm{Si}}/2,0)$ and at corner $P_{\mathrm{Corner}}=(t_{\mathrm{Si}}/2,t_{\mathrm{Si}}/2)$) results in

$$\overrightarrow{\nabla}\psi(P_{\mathrm{Half-side}})\cdot\hat{\imath}=\Omega\frac{V_G-\Delta\phi_{\mathrm{MS}}-\psi(P_{\mathrm{Half-side}})}{t_{\mathrm{Ox}}} \quad (4)$$

$$\overrightarrow{\nabla}\psi(P_{\mathrm{Corner}})\cdot\left(\frac{\hat{\imath}}{\sqrt{2}}+\frac{\hat{\jmath}}{\sqrt{2}}\right)=\Omega\frac{V_G-\Delta\phi_{\mathrm{MS}}-\psi(P_{\mathrm{Corner}})}{\sqrt{2}t_{\mathrm{Ox}}}. \quad (5)$$

We can use several holomorphic functions in (2), e.g., $\phi(z)=u(x,y)+\imath v(x,y)$, to generate different analytical expressions for the electric potential $\psi(x,y)$. One of the simplest could be $\phi_1(z)=mz$, where $m\in\mathbb{R}$ and $z=x+\imath y\in\mathbb{C}$.

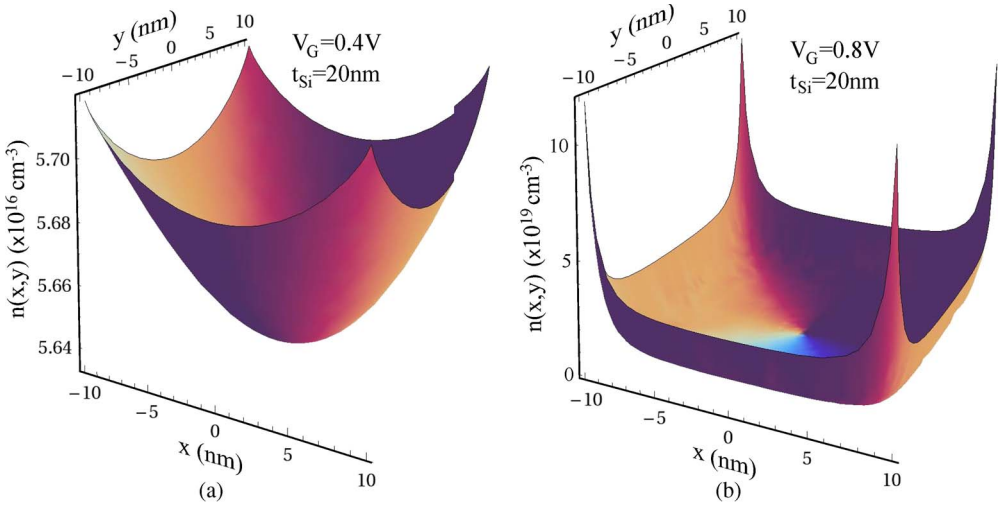

Fig. 2. Three-dimensional view of the simulated electron density for the square GAA MOSFET. The device technological parameters were the following: $t_{\mathrm{Si}} = 20$ nm, $t_{\mathrm{Ox}} = 1.5$ nm, $N_A = 10^{14}$ cm^{-3}, and $q\phi_m = 4.61$ eV. (a) $V_G = 0.4$ V. (b) $V_G = 0.8$ V.

By rewriting the previous holomorphic function as $\phi_1(z) = mz = u_1(x,y) + iv_1(x,y)$, we can conclude that $u_1(x,y) = mx$ and $v_1(x,y) = my$. Hence, we obtain $\phi_1'(z)\phi_1'^*(z) = (\partial u_1/\partial x)^2 + (\partial v_1/\partial x)^2 = m^2$ and $\phi_1(z)\phi_1^*(z) = u_1^2 + v_1^2 = m^2(x^2 + y^2)$. Putting all these results together in (2), an analytical solution for the electric potential is achieved as follows:

$$\psi_1(x,y) = \frac{1}{\beta}\ln\left(\frac{8m^2}{\alpha\beta\left(1 - m^2(x^2+y^2)\right)^2}\right). \tag{6}$$

$\psi_1(x,y)$ fulfills the Poisson equation (1). This function $\psi_1(x,y)$ was compared with the expression proposed in [10] as the electric potential for a cylindrical GAA MOSFET given by

$$\psi(r) = \frac{KT}{q}\ln\left(\frac{-8B}{\delta(1+Br^2)}\right). \tag{7}$$

After changing the Cartesian coordinate system to a cylindrical coordinate system $(x^2 + y^2 = r^2)$ and transforming a few constants ($B = -m^2$, $\delta = \alpha\beta$, and $\beta = q/KT$), it is easy to conclude that (6) and (7) are exactly the same expression. The electric potential shown in (7) worked well in developing an inversion-charge model for cylindrical GAA MOSFETs, as explained in [10]. Nevertheless, as will be shown below, the square GAA-MOSFET inversion-charge model based on $\psi_1(x,y)$ deals properly with only the subthreshold operation region.

The boundary conditions sketched above can be simplified in this case. Therefore, making use of (5), the following equation is obtained:

$$\left(\frac{\partial\psi_1}{\partial x}\left(\frac{t_{\mathrm{Si}}}{2},\frac{t_{\mathrm{Si}}}{2}\right)\hat{\imath} + \frac{\partial\psi_1}{\partial y}\left(\frac{t_{\mathrm{Si}}}{2},\frac{t_{\mathrm{Si}}}{2}\right)\hat{\jmath}\right)\left(\frac{\hat{\imath}}{\sqrt{2}} + \frac{\hat{\jmath}}{\sqrt{2}}\right) = \Omega\frac{V_G - \Delta\phi_{\mathrm{MS}} - \psi_1\left(\frac{t_{\mathrm{Si}}}{2},\frac{t_{\mathrm{Si}}}{2}\right)}{\sqrt{2}t_{\mathrm{Ox}}}. \tag{8}$$

Introducing (6) into (8), the following expression is found:

$$-\frac{4m^2 t_{\mathrm{Si}}}{\beta\left(m^2 2t_{\mathrm{Si}}^2 - 1\right)} = \frac{\Omega}{t_{\mathrm{Ox}}}\left(V_G - \Delta\phi_{\mathrm{MS}} - \frac{1}{\beta}\ln\left(\frac{8m^2}{\alpha\beta\left(\frac{1}{2}m^2 t_{\mathrm{Si}}^2 - 1\right)^2}\right)\right). \tag{9}$$

Parameter m can be obtained by solving (9) for different gate voltages V_G.

It is important to assess the appropriateness of the potential proposed by analyzing the inversion-charge distribution of the devices under study. Fig. 2 shows the simulated electron density corresponding to a $t_{\mathrm{Si}} = 20$ nm square GAA MOSFET. First, for gate voltages below the threshold voltage V_t, the variation in the electron density in the device is small [see Fig. 2(a)], and the corresponding potential distribution is quite flat. At high gate voltages [see Fig. 2(b)], where $V_G > V_t$, the inversion charge is close to the silicon–insulator interface, as expected in a MOSFET device. The corners are more inverted since the potential well there is deeper. It can be seen that, for an inversion-charge model to work properly in the strong-inversion operation region, it is essential to model the electric potential in the semiconductor perimeter reasonably well, and to do so, it is necessary to develop a model that shows a square shape at high gate voltages. When the inversion charge is placed at the semiconductor–insulator interface, i.e., showing a square shape (the inversion charge in the corners is important), a potential such as $\psi_1(x,y)$ (which shows cylindrical symmetry) would not be expected to fit numerical simulations.

It is clear that, in order to reproduce the electric potential in all the operation regions, a more complex function has to be used. To do this, other holomorphic functions were analyzed, which were inspired by conformal mapping techniques, to make the potential fit simulation data in such strongly

2-D geometry; from among these, the following one was chosen:

$$\phi_2(z)=mz+n\left(\frac{1}{z-\imath a}+\frac{1}{z+\imath a}-\frac{1}{z+a}-\frac{1}{z-a}\right) \quad (10)$$

with m, n, $a\in\mathbb{R}$, and $z\in\mathbb{C}$. ϕ_2 provides a reasonable trade-off between simplicity and accuracy and can be written as $\phi_2(x,y)=u_2(x,y)+\imath v_2(x,y)$, where $u_2(x,y)$ and $v_2(x,y)$ are given by

$$u_2(x,y)=n\left(\frac{x}{(y-a)^2+x^2}+\frac{x}{(a+y)^2+x^2}-\frac{x-a}{(x-a)^2+y^2}-\frac{a+x}{(a+x)^2+y^2}\right)+mx$$

$$v_2(x,y)=n\left(-\frac{y-a}{(y-a)^2+x^2}-\frac{a+y}{(a+y)^2+x^2}+\frac{y}{(x-a)^2+y^2}+\frac{y}{(a+x)^2+y^2}\right)+my.$$

A procedure similar to the one that followed to get (6) gives

$$\psi_2(x,y)=\frac{1}{\beta}\ln\left(\frac{8\left(m^2+\frac{\eta(x,y)+\varphi(x,y)}{(\omega(x,y))^2}\right)}{\alpha\beta\left(1-\frac{\xi(x,y)}{\omega(x,y)}\right)^2}\right) \quad (11)$$

where

$$\begin{aligned}
\omega(x,y)&=a^8-2a^4(x^4-6x^2y^2+y^4)+(x^2+y^2)^4\\
\eta(x,y)&=16a^4n^2\\
&\quad\times\left(a^8+6a^4(x^4-6x^2y^2+y^4)+9(x^2+y^2)^4\right)\\
\varphi(x,y)&=8a^2mn\\
&\quad\times\left(a^{12}+a^8(x^4-6x^2y^2+y^4)\right.\\
&\qquad-a^4\left(5x^8+52x^6y^2-34x^4y^4+52x^2y^6+5y^8\right)\\
&\qquad\left.+3(x^2+y^2)^4(x^4-6x^2y^2+y^4)\right)\\
\xi(x,y)&=(x^2+y^2)\\
&\quad\times\left(a^8m^2+8a^6mn\right.\\
&\qquad-2a^4\left(m^2(x^4-6x^2y^2+y^4)-8n^2\right)\\
&\qquad\left.-8a^2mn(x^4-6x^2y^2+y^4)+m^2(x^2+y^2)^4\right).
\end{aligned}$$

Because of the symmetry of the device under study, it can be deduced that the electric potential satisfies $\partial\psi/\partial x\rfloor_{(0,0)}=\partial\psi/\partial y\rfloor_{(0,0)}=0$ at the center point $P_{\text{Center}}=(0,0)$ (this point is indicated in Fig. 1). A first estimation of the m and n parameters was determined by making use of the boundary conditions (4) and (5). The a parameter controls the geometrical features of the electric potential since it fixes the divergence points of the four terms that are used to reproduce the square symmetry of the device structure model, as can be seen in (10). In this respect, we have chosen this parameter as part of a procedure within an heuristic approach to fit the simulation data.

As shown in Fig. 3, $\psi_2(x,y)$ reproduces the simulated electric potential for gate voltages below and above threshold and for different device sizes reasonably well (the m, n, and a parameters corresponding to each size and gate voltage can be found in Table I). It will be shown in the next section that this accuracy is good enough to reproduce the inversion charge (calculated by means of Gauss's law) for all the operation regions.

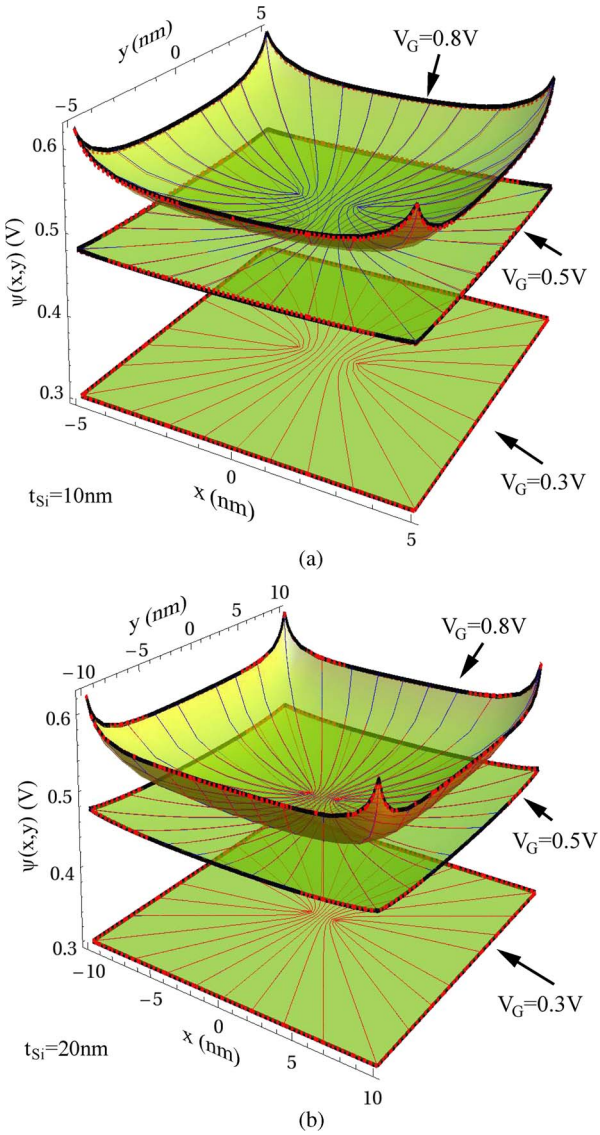

Fig. 3. Three-dimensional view of the electric potential for the square GAA MOSFET, with $t_{\text{Ox}}=1.5$ nm, $N_A=10^{14}$ cm^{-3}, and $q\phi_m=4.61$ eV. The modeled (simulated) data are represented by the surface with dashed (continuous) borders. (a) $t_{\text{Si}}=10$ nm. (b) $t_{\text{Si}}=20$ nm. The thin lines shown in the figure are perpendicular to the isopotential curves for each potential distribution.

TABLE I
FITTING PARAMETERS (m, n, AND a) USED FOR $\psi_2(x,y)$ IN FIGS. 3 AND 4

Size	Gate Voltage	$m\,(nm^{-1})$	$n\,(nm^{-1})$	$a\,(nm)$
10nm	0.3V	0.0059	0.0034	29
10nm	0.5V	0.935	0.059	13
10nm	0.8V	-6.226	0.015	12
20nm	0.3V	0.026	0.0033	58
20nm	0.5V	-9.007	-0.0159	30.56
20nm	0.8V	-12.8	0.018	22.3

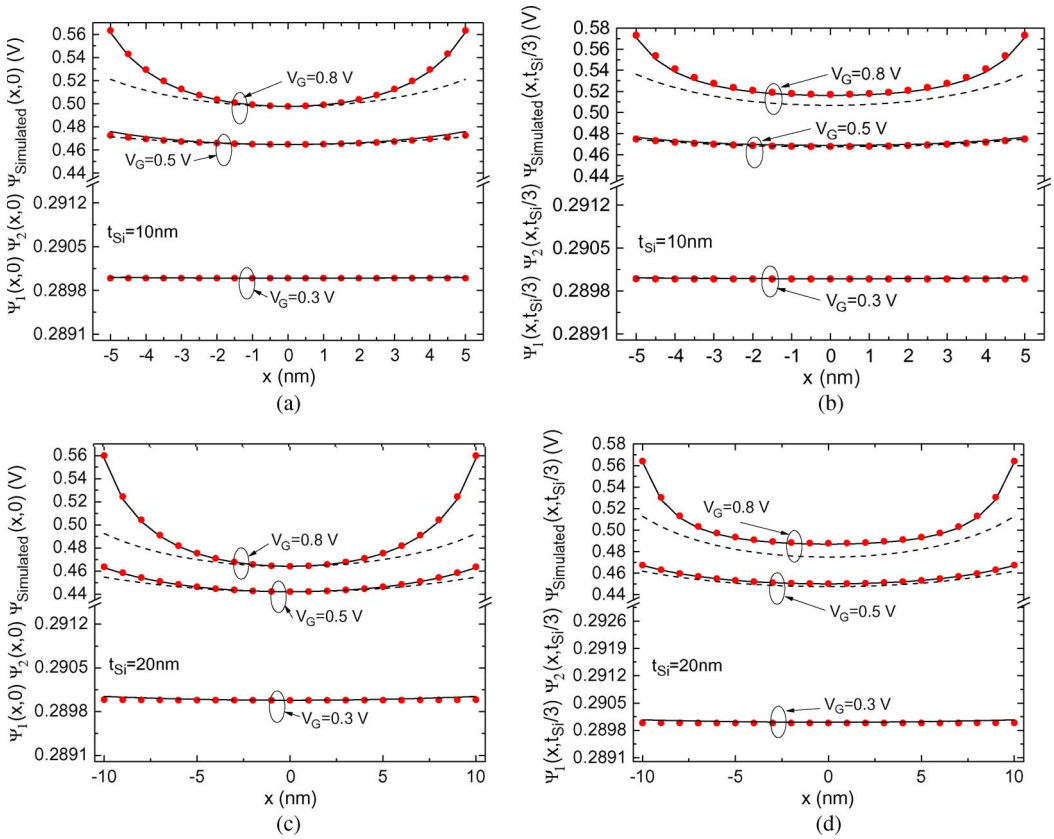

Fig. 4. Comparison of the electrical potential analytical functions (dashed line) ψ_1 and (solid line) ψ_2 with (circles) the simulated data along the x-coordinate of a GAA MOSFET. (a) $t_{\rm Si} = 10$ nm and $y = 0$. (b) $t_{\rm Si} = 10$ nm and $y = t_{\rm Si}/3$. (c) $t_{\rm Si} = 20$ nm and $y = 0$. (d) $t_{\rm Si} = 20$ nm and $y = t_{\rm Si}/3$.

In order to compare the accuracy of the two models developed, the potential distribution along the x-axis ($y = 0$ and $y = t_{\rm Si}/3$)) has been calculated using (6) and (11) and is shown in Fig. 4 together with the simulated data, for two different device sizes ($t_{\rm Si} = 10$ nm and $t_{\rm Si} = 20$ nm) and different gate voltages below and above the threshold voltage. As can be seen, both models fit the simulated data in the subthreshold-bias range accurately. At gate voltages close to the threshold voltage $V_G = 0.5$ V, the results achieved with (6) are accurate only for the smaller devices. This effect makes sense since the corners play a less important role for smaller $t_{\rm Si}$ and V_G values. However, at higher gate voltages, good agreement with the simulated data is attained only when $\psi_2(x, y)$ is considered, and the corners are quite important even for the smallest silicon width.

IV. Inversion-Charge Calculation

We have made use of Gauss's law to obtain the inversion charge of square GAA MOSFETs. The total inversion charge per unit length $Q_{\rm INV}$ was calculated by integrating the charge density in the silicon channel as follows:

$$Q_{\rm INV} = \int_{-\frac{t_{\rm Si}}{2}}^{\frac{t_{\rm Si}}{2}} \int_{-\frac{t_{\rm Si}}{2}}^{\frac{t_{\rm Si}}{2}} \rho(x,y)\,dx\,dy = 8\epsilon_{\rm Si} \int_0^{\frac{t_{\rm Si}}{2}} -\frac{\partial\psi(x,y')}{\partial x}\bigg|_{x=-\frac{t_{\rm Si}}{2}} dy'. \quad (12)$$

The symmetry of the device under study was used on the right-hand side of (12), and the integral of the electric field along the GAA MOSFET silicon–insulator interface was calculated.

By making use of $\psi_1(x, y)$ defined in (6), the electric field can be calculated as follows:

$$-\frac{\partial\psi_1}{\partial x}\left(\frac{t_{\rm Si}}{2}, y\right) = \frac{2m^2 t_{\rm Si}}{\beta\left(m^2\left(\frac{t_{\rm Si}^2}{4} + y^2\right) - 1\right)}. \quad (13)$$

Therefore, the expression for the inversion charge per unit of length was in this case given by

$$Q_{\rm INV} = -\frac{32 m t_{\rm Si}\varepsilon_{\rm Si}\arctan\left(\frac{m t_{\rm Si}}{\sqrt{m^2 t_{\rm Si}^2 - 4}}\right)}{\beta\sqrt{m^2 t_{\rm Si}^2 - 4}}. \quad (14)$$

The inversion charge calculated through (14) was compared with simulated data (see Fig. 5) for GAA MOSFETs with different silicon channel thicknesses. It can be concluded that this model reproduces accurately the inversion charge in the subthreshold operation region but not in the strong-inversion regime, as was expected.

Subsequently, $\psi_2(x, y)$ was also used to calculate the inversion charge by means of (12). In this case, the analytical expression obtained for the inversion charge is much more complex than (14). Fig. 6 shows the modeled inversion-charge data compared with the simulations. In this case, a good fit is obtained for the gate voltage range considered in this paper,

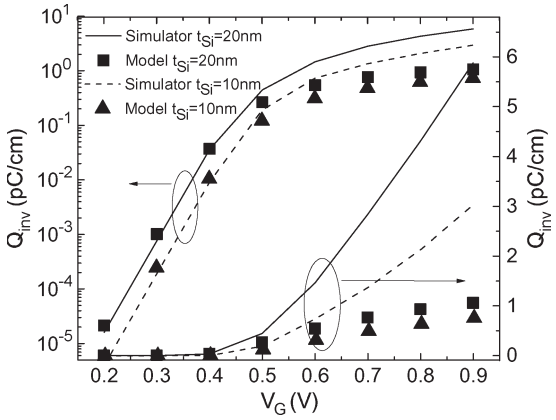

Fig. 5. Inversion charge versus gate voltage for a square GAA MOSFETs with different $t_{\rm Si}$ values. Simulation data are shown in lines ($t_{\rm Si} = 20$ nm is shown in solid lines and $t_{\rm Si} = 10$ nm is shown in dashed lines), and modeled data (for $\psi_1(x, y)$) are plotted in symbols ($t_{\rm Si} = 20$ nm is shown in squares and $t_{\rm Si} = 10$ nm is shown in triangles).

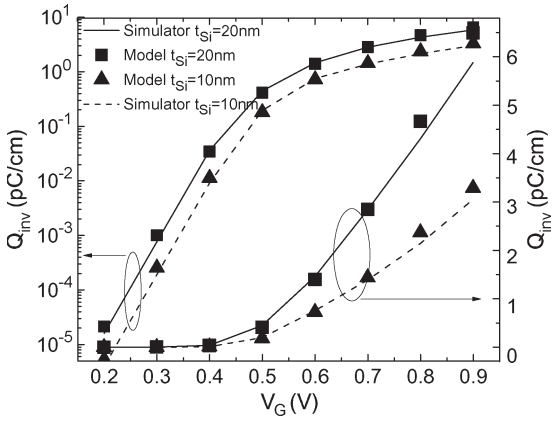

Fig. 6. Inversion charge versus gate voltage for a square GAA MOSFET with different $t_{\rm Si}$ values. Simulation data are shown in lines ($t_{\rm Si} = 20$ nm is shown in solid lines and $t_{\rm Si} = 10$ nm is shown in dashed lines) and modeled data (for $\psi_2(x, y)$) are plotted in symbols ($t_{\rm Si} = 20$ nm is shown in squares and $t_{\rm Si} = 10$ nm is shown in triangles).

including the subthreshold operation regime, and for the two silicon layer thicknesses taken into account.

V. Conclusion

This paper has presented a new approach to the analytical solution of the 2-D Poisson equation in undoped square GAA MOSFETs, including the inversion-charge density in the silicon channel. Using this approach, different sets of solutions can be chosen to model the potential in such complex devices.

Specifically, we have considered two tentative potential functions with different degrees of complexity. First, we have proven that a potential that can also be used for cylindrical GAA MOSFETs satisfies the Poisson equation for square ones. However, the results achieved for inversion-charge modeling are accurate only in the subthreshold region, where the charge is not confined strongly close to the oxide interface. The second more complicated function for the potential, which can model accurately both the potential distribution and the inversion charge, has then been introduced.

The potential functions we have presented for square GAA MOSFETs therefore could be useful to develop new compact models. Finally, we would like to highlight that the mathematical approach presented here can be used to find other potential distributions, allowing a higher degree of accuracy in the modeling of the devices.

Appendix A

Equation (1) can be rewritten as follows for simplicity:

$$\Delta\psi(x, y) = \alpha e^{\beta\psi(x,y)} \tag{15}$$

where $\alpha = (q/\epsilon_{\rm Si})n_i$ and $\beta = q/KT$.

In order to find an analytical solution to this equation, we determinate the general solution of (15), which is a particular case of the following equation:

$$\Delta\psi(x, y) = \epsilon f(x, y)e^{\beta\psi(x,y)} \tag{16}$$

This equation has been solved analytically by following an approach similar to [19]. The following expression has been obtained for the following potential:

$$\psi(x, y) = -\frac{2}{\beta}\ln\left(\frac{\sqrt{\frac{|\beta|}{2}}\,|F(z)|\,(1-\varepsilon\cdot\mathrm{sgn}\beta\phi(z)\phi^*(z))}{2\,|\phi'(z)|}\right) \tag{17}$$

where F is a holomorphic function[1, 2] such that $|F(z)|^2 = f(x, y)$, $\epsilon = \pm 1$, and $\phi(z)$ is an arbitrary holomorphic function with a nonvanishing derivative.

Since (15) is obtained from (16) for $\epsilon = +1$ and $f(x, y) = \alpha > 0$, we get the following expression for the general solution of (15):

$$\begin{aligned}\psi(x, y) &= -\frac{2}{\beta}\ln\left(\frac{\sqrt{\frac{\alpha\beta}{2}}\,(1-\phi(z)\phi^*(z))}{2\,|\phi'(z)|}\right)\\ &= \frac{1}{\beta}\ln\left(\frac{8\phi'(z)\phi'^*(z)}{\alpha\beta\,(1-\phi(z)\phi^*(z))^2}\right)\end{aligned} \tag{18}$$

References

[1] International Technology Roadmap for Semiconductors, 2009. [Online]. Available: http://www.itrs.net

[2] A. Vandooren, "Multiple gates and strained films for SOI MOSFETs," in *Proc. 2nd Workshop Thematic Netw. Silicon Insulator Technol., Devices Circuits—EUROSOI*, Grenoble, France, 2006.

[3] J. P. Colinge, "Multiple-gate SOI MOSFETs," *Solid State Electron.*, vol. 48, no. 6, pp. 897–905, Jun. 2004.

[1] A holomorphic function is a complex-valued function of one or more complex variables that is complex differentiable in a neighborhood of every point in its domain. The phrase "holomorphic at point z_0" means not just differentiable at z_0 but differentiable everywhere within some neighborhood of z_0 in the complex plane. If U is an open subset of the complex plane $\mathbb{C}$, then function $\phi : U \to \mathbb{C}$ is holomorphic, and its derivative is nonzero everywhere on U if and only if it is conformal (or angle preserving) at u_0 and if it preserves oriented angles between curves through u_0 in terms of their orientation [20].

[2] If the complex function $\phi(z) = u(x, y) + \imath v(x, y)$ (where $z = x + \imath y \in \mathbb{C}$) is holomorphic, then $u(x, y)$ and $v(x, y)$ first partial derivatives with respect to x and y exist and satisfy the Cauchy–Riemann equations $\partial u/\partial x = \partial v/\partial y$ and $\partial u/\partial y = -\partial v/\partial x$. [20]

[4] A. Craig, G. Roy, and A. Asenov, "Random-dopant-induced drain current variation in nano-MOSFETs: A three dimensional self-consistent Monte Carlo simulation study using "ab initio" ionized impurity scattering," *IEEE Trans. Electron Devices*, vol. 55, no. 11, pp. 3251–3258, Nov. 2008.
[5] G. Celler and S. Cristoloveanu, "Frontiers of silicon-on-insulator," *J. Appl. Phys.*, vol. 93, no. 9, pp. 4955–4978, May 2003.
[6] M. F. Bukhori, S. Roy, and A. Asenov, "Simulation of statistical aspects of charge trapping and related degradation in bulk MOSFETs in the presence of random discrete dopants," *IEEE Trans. Electron Devices*, vol. 57, no. 4, pp. 795–803, Apr. 2010.
[7] J. P. Colinge, *Silicon-on-Insulator Technology: Materials to VLSI*, 3rd ed. Norwell, MA: Kluwer, 2004.
[8] O. Moldovan, B. Iniguez, D. Jiménez, and J. Roig, "Analytical charge and capacitance models of undoped cylindrical surrounding-gate MOSFETs," *IEEE Trans. Electron Devices*, vol. 54, no. 1, pp. 162–165, Jan. 2007.
[9] J. Roldán, A. Godoy, F. Gámiz, and M. Balaguer, "Modeling the centroid and the inversion charge in cylindrical surrounding gate MOSFETs, including quantum effects," *IEEE Trans. Electron Devices*, vol. 55, no. 1, pp. 411–416, Jan. 2008.
[10] D. Jiménez, B. Iniguez, J. Suné, L. F. Marsal, J. Pallarés, J. Roig, and D. Flores, "Continuous analytic I–V model for surrounding-gate MOSFETs," *IEEE Electron Device Lett.*, vol. 25, no. 8, pp. 571–573, Aug. 2004.
[11] H. Cho and J. Plummer, "Modeling of surrounding gate MOSFETs with bulk trap states," *IEEE Trans. Electron Devices*, vol. 54, no. 1, pp. 166–169, Jan. 2007.
[12] S. Oh, D. Monroe, and J. M. Hergenrothe, "Analytic description of short channel effects in fully-depleted double-gate and cylindrical surrounding gate MOSFETs," *IEEE Electron Device Lett.*, vol. 21, no. 9, pp. 445–447, Sep. 2000.
[13] E. Gnani, S. Reggiani, M. Rudan, and G. Baccarani, "A new approach to the self-consistent solution of the Schrödinger-Poisson equations in nanowire MOSFETs," in *Proc. ESSDERC*, 2004, pp. 177–180.
[14] R. Ritzenthaler, F. Lime, B. Iñiguez, O. Faynot, and S. Cristoloveanu, "3D analytical modelling of subthreshold characteristics in Pi-gate FinFET transistors," in *Proc. ESSDERC*, 2010, pp. 448–451.
[15] A. Godoy, A. R. Gallardo, C. Sampedro, and F. Gámiz, "Quantum mechanical effects in multiple gates MOSFETs," *J. Comput. Electron.*, vol. 6, no. 1–3, pp. 145–148, Sep. 2007.
[16] F. G. Ruiz, A. Godoy, F. Gámiz, C. Sampedro, and L. Donetti, "A comprehensive study of the corner effects in pi-gate MOSFETs including quantum effects," *IEEE Trans. Electron Devices*, vol. 55, no. 12, pp. 3369–3377, Dec. 2007.
[17] B. Iniguez, D. Jiménez, J. Roig, H. A. Hamid, L. F. Marsal, and J. Pallarés, "Explicit continuous model for long-channel undoped surrounding gate MOSFETs," *IEEE Trans. Electron Devices*, vol. 52, no. 8, pp. 1868–1873, Aug. 2005.
[18] Y. Taur, "Analytic solutions of charge and capacitance in symmetric and asymmetric Double-Gate MOSFETs," *IEEE Trans. Electron Devices*, vol. 48, no. 12, pp. 2861–2869, Dec. 2001.
[19] I. K. Sabitov, "Solutions of $\delta u = \epsilon f(x; y)e^{cu}$ in some special cases," *Sbornik: Math.*, vol. 192, no. 6, pp. 879–984, 2001.
[20] E. Kreyszig, *Advanced Engineering Mathematics*, 9th ed. Hoboken, NJ: Wiley, 2006.

Enrique Moreno Pérez received the B.S. degree in applied physics and instrumentation from Cork Institute of Technology, Cork, Ireland, in 2008, and the M.S. degrees in fundamental physics and in advanced methods and techniques in physics in 2009 and 2010, respectively, from the Universidad de Granada, Granada, Spain, where he is currently working toward the Ph.D. degree in physics in the Group of Electromagnetics of Granada.

He worked on avalanche photodiodes characterization in the Photonic Department, Tyndall National Institute, Cork, and on the study and modeling of gate-all-around metal–oxide–semiconductor field-effect transistors in the Department of Electronics, Universidad de Granada. His main research interest concerns photoconductive antennas in the terahertz range.

Juan Bautista Roldán Aranda received the M.S. degree in physics and the Ph.D. degree from the Universidad de Granada, Granada, Spain, in 1993 and 1997, respectively.

He is currently an Associate Professor with the Universidad de Granada. Since 1993, he has been working on MOS device physics, including Monte Carlo transport simulations and compact modeling. Among other topics, he has been involved in the study and modeling of strained-Si and silicon-on-insulator (SOI) and SiC MOS field-effect transistors. He has coauthored more than 60 refereed technical journal papers and 70 communications at international conferences. His current research interest includes modeling of nanometric conventional and multigate devices mainly based on SOI technology and Verilog-A implementation of device models for circuit simulation.

Francisco J. García Ruiz received the M.Sc. degree in telecommunication engineering from the University of Málaga, Málaga, Spain, and the Ph.D. degree from the University of Granada, Granada, Spain, in 2002 and 2005, respectively.

From 2001 to 2006, he was with the Group of Electromagnetics of Granada, University of Granada. He was a Visiting Researcher at the IRCTR, Delft, The Netherlands, in 2005. He is currently with the Department of Electronics, University of Granada, as an Assistant Professor. His research interests include numerical methods applied to the simulation of electron devices.

Domingo Barrera Rosillo received the M.S. degree in mathematics and the Ph.D. degree from the Universidad de Granada, Granada, Spain.

He is currently an Associate Professor with the Universidad de Granada. Since 1997, he has been working on multivariate approximation, numerical analysis, and spline interpolation and quasi-interpolation. He is collaborating with different groups of the electronics engineering and civil engineering departments, applying numerical methods for the solution of several problems arising in those areas. His current research interest also includes numerical solution of partial differential equations by spline-based methods.

Prof. Barrera Rosillo is a Coorganizer of the International Conference on Approximation Methods and Numerical Modeling in Environment and Natural Resources, which is a biennial meeting sponsored by IMACS, and a Guest Editor for the special issues published by Mathematics and Computers in Simulation.

María José Ibáñez Pérez received the M.S. degree in mathematics and the Ph.D. degree from the Universidad de Granada, Granada, Spain.

She is currently an Associate Professor with the Departamento de Matemática Aplicada, Universidad de Granada. Since 2000, she has been working on multivariate approximation, numerical analysis, and spline quasi-interpolation. Her current research interest also includes subdivision methods for curves and surfaces.

Prof. Ibáñez Pérez is collaborating with the nanoelectronic research group and the approximate reasoning and artificial intelligence research group of the Universidad de Granada and coorganizes the International Conference on Approximation Methods and Numerical Modeling in Environment and Natural Resources, which is a biennial meeting sponsored by IMACS.

Andrés Godoy (M'08) received the B.S. and Ph.D. degrees in physics from the University of Granada, Granada, Spain, in 1993 and 1997, respectively.

He is currently an Associate Professor with the University of Granada. He was a Visiting Researcher at the Beckman Institute, University of Illinois, Urbana-Champaign. His current research interests include Monte Carlo simulation of semiconductor devices, noise modeling, and nanoelectronics.

Francisco Gámiz received the B.S. degree in physics and the Ph.D. degree from the University of Granada, Granada, Spain, in 1991 and 1994, respectively.

Since 1991, he has been working on the characterization of scattering mechanisms and their influence on the transport properties of charge carriers in semiconductor heterostructures. In 1999, he was a Visiting Researcher at the IBM T.J. Watson Research Center, Yorktown Heights, NY. Since April 2005, he has been a Professor of electronics with the University of Granada. He has studied electron mobility in silicon inversion layers by the Monte Carlo method. His current research interests include the effects of many carriers on electron mobility and the theoretical interpretation of the influence of high longitudinal electric fields on the electrical properties of metal–oxide–semiconductor transistors. His other interests are related to SiGe and SiC, silicon-on-insulator and germanium-on-insulator devices, and quantum transport. He has coauthored more than 100 refereed papers in all these subjects.

Prof. Gámiz is the Coordinator of EUROSOI European Network on Silicon-on-Insulator Technology, Devices and Systems.